Short - 45

74

DR-865

LA-5618-MS

Informal Report

UC-28
Reporting Date: April 1974
Issued: May 1974

Slit Scattering in the EPICS Beam Line

by

Norbert Ensslin*
H. A. Thiessen

*Guest Scientist. Permanent address: University of Colorado, Boulder, CO.

los alamos
scientific laboratory
of the University of California
LOS ALAMOS, NEW MEXICO 87544

UNITED STATES
ATOMIC ENERGY COMMISSION
CONTRACT W-7405-ENG. 36

In the interest of prompt distribution, this LAMS report was not edited by the Technical Information staff.

Printed in the United States of America. Available from
National Technical Information Service
U. S. Department of Commerce
5285 Port Royal Road
Springfield, Virginia 22151
Price: Printed Copy $4.00; Microfiche $1.45

SLIT SCATTERING IN THE EPICS BEAM LINE

by

Norbert Ensslin and H. A. Thiessen

ABSTRACT

A Monte Carlo calculation of the interaction of charged particles with collimating slits was used to simulate the EPICS channel and spectrometer. The program was applied to the design of collimating jaws for the channel and to the selection of event rejection tests for the spectrometer. It was possible to predict the expected backgrounds of muons, protons, and slit-scattered pions.

I. DESCRIPTION OF PROGRAM

Particles emanating from a target are simulated by choosing rays of random position and angle with respect to a common origin. The rays are traced through a series of slits, which may be collimating jaws, vacuum pipes, or magnet pole tips. The slits may have rectangular or elliptical apertures, and may be straight, sloping, or parabolic in cross section.

Composition of the slits is determined by specifying the radiation length, collision length, and energy loss of minimum ionizing pions. The values used are listed in Table I.

TABLE I

ATOMIC AND NUCLEAR PROPERTIES OF SLIT MATERIALS*

Material	Z	Radiation Length cm	Collision Length (Hadrons) cm	Minimum dE/dx MeV/cm
C	6	18.9	26.8	4.00
Al	13	8.86	29.3	1.66
Fe	26	1.44	11.8	12.9
W	74	0.36	7.8	22.6
U	92	0.29	8.75	20.5

* From N. Barash-Schmidt et al., "Review of Particle Properties," UCRL-8030, 1969.

While the particle is inside the slit material, it is stepped through in steps that are initially 1 mm in size, but which increase gradually to about 1 cm. At each step, the particle is allowed to scatter about its direction of motion. The angle of scatter is chosen randomly from a gaussian distribution of standard deviation

$$\sqrt{<\theta^2>} = 21.3 \frac{E}{p^2} \sqrt{\frac{t}{t_{rad}}} \quad ,$$

where $\underline{E}$ = total energy (MeV), $\underline{p}$ = momentum (MeV), and t/t_{rad} is the distance traveled, in radiation lengths. The collision length allows for the random removal of pions due to nuclear interactions without considering specific reactions. As the particle moves through the material, its energy is progressively reduced. If the multiple scattering or energy loss becomes excessive, the particle is discarded. If a step carries the ray out of the slit material, it is first traced back to the boundary before proceeding.

The values in Table I were also used for muons and protons, with two exceptions. Since muons do not interact strongly with nuclei, no collision length was used. Since protons are not minimum-ionizing in the range of momenta covered by EPICS, larger values of dE/dx were used.[1]

MASTER

Thin lenses can be introduced at any boundary between two slits. They are of the form

$$\begin{pmatrix} x \\ \frac{dx}{dz} \\ \delta \end{pmatrix} = \begin{pmatrix} 1 & 0 & 0 \\ -1/f_x & 1 & D_x \\ 0 & 0 & 1 \end{pmatrix} \begin{pmatrix} x_o \\ \frac{dx}{dz}_o \\ \delta_o \end{pmatrix} ,$$

where x is the transverse displacement, z is the distance along the central ray, δ is the deviation in momentum from the central ray, f is the focal length, and D is the angular dispersion. The matrix elements correspond to the dominant first-order coefficients used by the computer code TRANSPORT[2], with the exception that θ is replaced by tan θ.

The random decay of pions into muons and neutrinos is allowed for. In the rest frame of the pion, the direction of the emitted muon is chosen randomly. Also considered is the decay of muons into electrons, but since this occurs relatively infrequently and involves a three-body final state, the kinematics are treated only approximately.

It would be possible to simulate the interaction physics or the magnet optics more accurately. However, as much computer time as possible is devoted to simulating the scattering of particles which strike slits at grazing angles. This is done by using smaller step sizes near the edges of the slit and by using step sizes as small as practical. Figure 1 shows the results of a test to determine the step size needed. Pions of 200 MeV kinetic energy were allowed to strike a large, slightly curved uranium jaw at grazing incidence, as illustrated in Fig. 2. The energy distribution of the pions that re-emerge from the slit is difficult to predict exactly, but it should be a rapidly decreasing function of energy, with perhaps a long tail. Figure 3 yields such a shape for sufficiently small step sizes. Although 0.25 mm appears to be significantly better than 1.0 mm in this test, both sizes were found to give essentially the same results in simulating the EPICS channel. Also, a 1.0-mm step was found to be the smallest practical size in terms of running times.

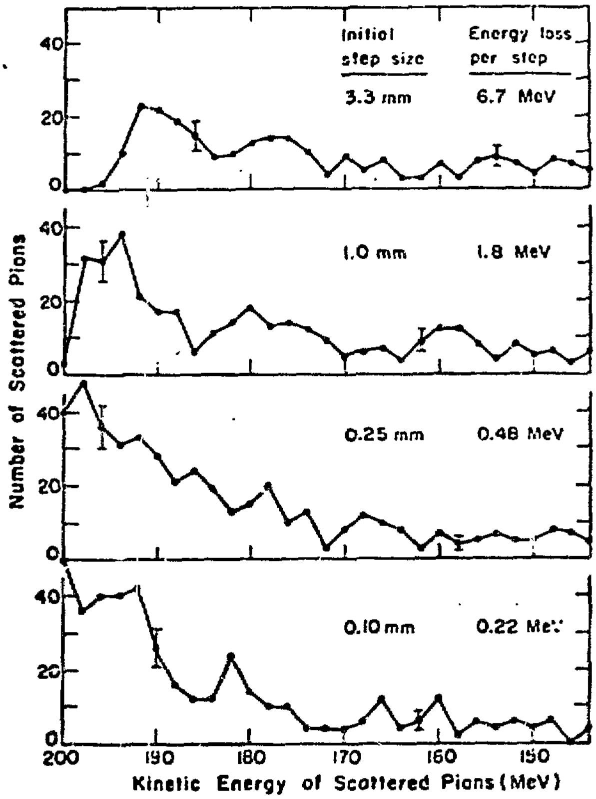

Fig. 1. Energy distribution of slit-scattered pions as a function of step size inside slit.

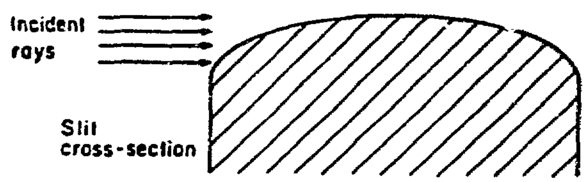

Fig. 2. Geometry of single slit tests.

The program employs two independent random number generating sequences. One is used to generate new rays, the other to trace them through slits. Use of the same set of initial rays can reduce statistical uncertainties in cases where it is necessary to study the effect of a small change in slit geometry.

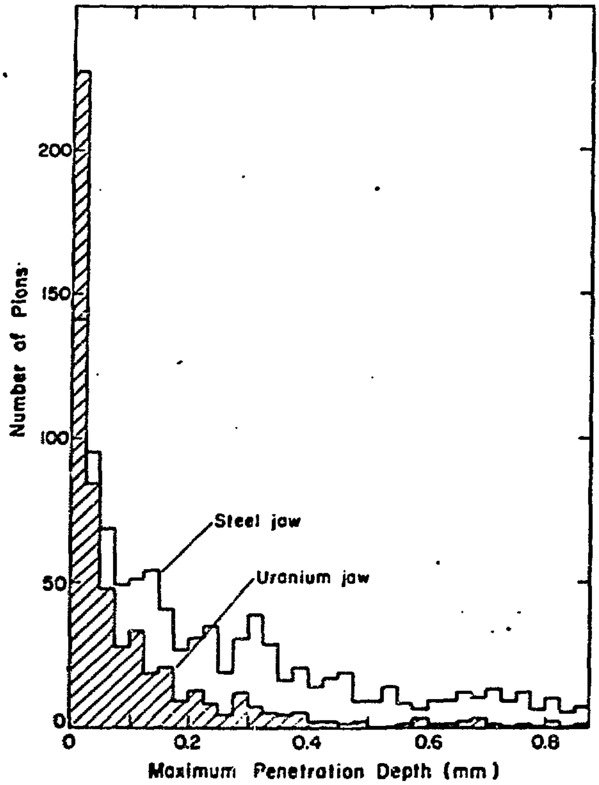

Fig. 3. Distribution of the maximum depth attained by pions which re-emerged from a slit. Two-thirds of the pions penetrated to depths of less than 0.1 mm in U, 0.5 mm in steel.

II. SINGLE SLIT RESULTS

Initial tests with a single slit, as in Fig. 2, showed that the best collimation of an incident beam is obtained with slightly curved jaws of high Z material. High Z increases the energy loss, collision loss, and multiple scattering of a particle which enters the slit. This increases the probability that the particle will be absorbed or at least scattered out of the beam. A small curvature (about 50-cm radius) was found to be more effective than a flat surface. This was true even for a perfectly parallel incident beam, where there was no possibility of particles passing through a corner of the slit. A small curvature allows particles to strike the slit at a larger angle, which apparently makes it more difficult for them to scatter out again.

It was found that about 1/3 of the particles which struck the slit re-emerged. Most of these had penetrated to depths of only 0.1 - 0.5 mm into the slit, as illustrated in Fig. 3. This implies that a coating of higher Z or lower Z material can significantly alter the properties of a slit. Although many particles re-emerged, only 10^{-3} scattered back into the phase space of a "target" positioned downstream. In order to determine if this ratio would be substantially increased by double or triple scatterings if there were other slits farther downstream, a study of the full EPICS channel was undertaken.

III. EPICS CHANNEL SIMULATION

The EPICS channel consists of four 52.5° bending magnets and ten pairs of moveable steel or uranium jaws. These must select pions of a given energy range and collimate them into a beam at the scattering target. Figure 4 illustrates the positions of the slits and lenses used to simulate the channel, and Table II lists the dimensions and focal lengths. In the horizontal plane, the optics are point-to-parallel, with crossed E and B fields after the first magnet to separate protons. In the vertical plane, the optics are point-to-point, with 9.2 cm/% dispersion at the scattering target.

Horizontal focussing is accomplished only by the fringe fields at the entrance and exit of the magnets. The focal lengths of the equivalent thin lenses are[2]

$$\frac{1}{f_y} = \frac{\tan\,(\beta - \psi)}{\rho} \quad ,$$

$$\psi = \frac{1 + \sin^2\beta}{\beta}\left[k_1\left(\frac{g}{\rho}\right) - k_2\left(\frac{k_1 g}{\rho}\right)^2 \tan\beta\right]$$

where $k_1 = 0.4$, $k_2 = 4.4$ (clamped Rogowski fringing field), $g/2 = 4.445$ cm (half aperture of magnet), $\rho = 76.40$ cm (radius of curvature of the central trajectory), and β is the angle of the pole face with the normal to the central trajectory. ψ is the correction to β produced by the fringing fields. Because of the fringing fields, these lenses should actually be positioned near the effective field boundary. However, it was possible to reproduce the first-order optics and the beam envelope to within 5-10% with the lenses positioned at the actual pole boundaries.

The production target was simulated by choosing rays randomly over a 0.2-cm interval in the vertical direction, and over a 3.0-cm interval along the

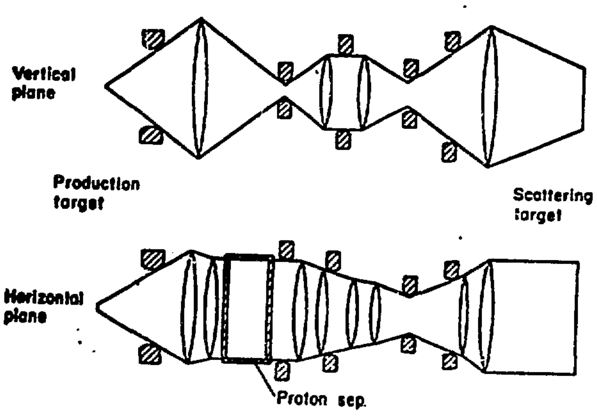

Fig. 4. EPICS channel slits and lenses.

proton beam. In the horizontal direction, a gaussian distribution with a standard deviation of 1.0 cm was used to choose rays. This distribution reproduces the proton beam profile in the horizontal direction, but the width has been increased to simulate in part the higher order aberrations in the channel optics. These initial coordinates were then rotated by 35° and projected down the channel. The initial phase space was chosen large enough to include all rays with a reasonable chance of scattering into the acceptance of the channel.

Pions and protons were started into the channel in this manner. They were traced through all of the

TABLE IIA

EPICS CHANNEL SLITS

ZA, ZB define the position of the slit along the central trajectory. The half-aperture is $A + ZSLP(Z - ZC) + (Z - ZC)^2/2RC$.

Composition		ZA	ZB	ZC(X)	ZC(Y)	ZSLP(X)	ZSLP(Y)	RC(X)	RC(Y)	A(X)	A(Y)
1	Fe	15.20	38.10	38.10	38.10	.0555	.0555	0.000	0.000	5.080	5.080
2	Fe	38.10	38.30	38.30	38.30	.0750	.0750	0.000	0.000	3.830	3.830
3	Fe	38.30	49.80	49.80	49.80	0.0000	0.0000	0.000	0.000	10.000	5.000
4	W	49.80	68.90	68.90	68.90	0.0000	.0094	0.000	0.000	5.556	2.169
5	W	68.90	76.90	68.90	68.90	0.0000	.0094	45.720	45.720	5.556	2.169
6	Fe	76.90	137.20	76.90	76.90	0.0000	0.0000	0.000	0.000	16.000	5.000
7	U	137.20	162.60	149.90	149.90	0.0000	0.0000	50.000	50.000	11.200	5.000
8	Fe	162.60	165.10	162.60	162.60	0.0000	0.0000	0.000	0.000	30.000	5.000
9	U	165.10	190.50	177.80	177.80	0.0000	0.0000	50.000	50.000	50.000	3.400
10	Fe	190.50	292.50	190.50	190.50	0.0000	0.0000	0.000	0.000	50.000	5.000
11	Fe	292.50	302.50	302.50	302.50	0.0000	0.0000	0.000	10.000	40.000	4.445
12	Fe	302.50	352.50	302.50	302.50	0.0000	0.0000	0.000	0.000	40.000	4.445
13	Fe	352.50	362.50	352.50	352.50	0.0000	0.0000	0.000	10.000	40.000	4.445
14	Fe	362.50	565.50	565.50	565.50	0.0000	0.0000	0.000	0.000	50.000	5.000
15	U	565.50	573.00	568.90	0.00	0.0000	0.0000	25.000	0.000	2.000	5.000
16	Fe	573.00	590.50	590.50	590.50	0.0000	0.0000	0.000	0.000	50.000	5.000
17	U	590.50	595.50	0.00	593.00	0.0000	0.0000	0.000	50.000	50.000	4.445
18	Fe	595.50	642.10	642.10	642.10	0.0000	0.0000	0.000	0.000	50.000	5.000
19	Fe	642.10	652.10	652.10	652.10	0.0000	0.0000	0.000	10.000	30.000	4.445
20	Fe	652.10	702.10	702.10	702.10	0.0000	0.0000	0.000	0.000	30.000	4.445
21	Fe	702.10	712.10	702.10	702.10	0.0000	0.0000	0.000	10.000	30.000	4.445
22	Fe	712.10	734.60	734.60	734.60	0.0000	0.0000	0.000	0.000	50.000	5.000
23	Fe	734.60	739.60	737.10	737.10	0.0000	0.0000	0.000	0.000	50.000	5.000
24	Fe	739.60	762.10	762.10	762.10	0.0000	0.0000	0.000	0.000	50.000	5.000
25	Fe	762.10	767.10	764.60	764.60	0.0000	0.0000	0.000	0.000	13.000	5.000
26	Fe	767.10	812.10	812.10	812.10	0.0000	0.0000	0.000	0.000	50.000	5.000
27	Fe	812.10	822.10	822.10	822.10	0.0000	0.0000	0.000	10.000	30.000	4.445
28	Fe	822.10	872.10	872.10	872.10	0.0000	0.0000	0.000	0.000	30.000	4.445
29	Fe	872.10	882.10	872.10	872.10	0.0000	0.0000	0.000	10.000	30.000	4.445
30	Fe	882.10	954.40	954.40	954.40	0.0000	0.0000	0.000	0.000	50.000	5.000
31	U	954.40	964.40	960.90	0.00	0.0000	0.0000	50.000	0.000	5.000	5.000
32	Fe	964.40	981.10	981.10	981.10	0.0000	0.0000	0.000	0.000	50.000	5.000
33	U	981.10	996.10	0.00	988.60	0.0000	0.0000	0.000	50.000	50.000	1.700
34	Fe	996.10	1094.00	1094.00	1094.00	0.0000	0.0000	0.000	0.000	50.000	5.000
35	U	1094.00	1109.00	1100.00	0.00	0.0000	0.0000	50.000	0.000	16.000	5.000
36	Fe	1109.00	1118.00	1118.00	1118.00	0.0000	0.0000	0.000	0.000	50.000	5.000
37	U	1118.00	1133.00	0.00	1125.00	0.0000	0.0000	0.000	50.000	50.000	3.000
38	Fe	1133.00	1162.00	1162.00	1162.00	0.0000	0.0000	0.000	0.000	50.000	5.000
39	Fe	1162.00	1172.00	1172.00	1172.00	0.0000	0.0000	0.000	10.000	40.000	4.445
40	Fe	1172.00	1222.00	1222.00	1222.00	0.0000	0.0000	0.000	0.000	40.000	4.445
41	Fe	1222.00	1232.00	1222.00	1222.00	0.0000	0.0000	0.000	10.000	40.000	4.445
42	Fe	1232.00	1524.00	1524.00	1524.00	0.0000	0.0000	0.000	0.000	50.000	5.000

TABLE IIB

EPICS CHANNEL LENSES

N	-1/fx	-1/fy	DX	DY
11	0.0000000	-.003482[illegible]	0.000	0.000
12	-.0071051	0.0000000	7.100	0.000
14	0.0000000	.0013365	0.000	0.000
19	0.0000000	-.0033942	0.000	0.000
21	-.0073206	0.0000000	-10.160	0.000
22	0.0000000	.0036047	0.000	0.000
27	0.0000000	.0036047	0.000	0.000
28	-.0073206	0.0000000	-10.160	0.000
30	0.0000000	-.003390[illegible]	0.000	0.000
39	0.0000000	.0013365	0.000	0.000
41	-.0071042	0.0000000	16.750	0.000
42	0.0000000	-.0048217	0.000	0.000

The lenses are positioned between slits N, N-1.

---

slits and lenses, as described in Part I. The pions, slit-scattered pions, muons, and protons which emerged were required to pass through the 20-cm by 8.89-cm area covered by the scattering target. Slit scattered pions were found to comprise 0.1% of all pions passed, in accord with the single slit results described earlier.

Since optical aberrations are quite large in the channel (about 1/2-cm spot size at the crossovers), the above result seemed unrealistically small. Two methods of simulating the channel aberrations were tried. Firstly, each pair of jaws was set to intercept 5% of the beam envelope defined by the preceding pair. This method yielded a background of 0.2% slit-scattered pions. Secondly, each lens was made to fluctuate slightly in strength for every pion by adding a small random number to the focal length. The random number was chosen from a gaussian distribution, whose width was set to reproduce the 1/2-cm displacements mentioned above. This method yielded a background of 0.4%.

Incident pions of momentum lower than the acceptance of the channel were not passed. Pions of higher momentum, up to 35% higher, contributed an additional 0.2% scattered pions to the 0.4% or less described above. The 0.6% slit-scattered pions cannot be distinguished by the spectrometer, and will produce a background at the focal plane.

This background appears to be concentrated at the positions of the regular peaks. In other words, most slit-scattered pions strike the target close to the position expected on the basis of the 9.2 cm/% dispersion of the channel. As illustrated in Fig. 5, histograms of unscattered pions and scattered pions have nearly identical widths of 3×10^{-3} and 4×10^{-3}, respectively. Of course, the resolution of the actual channel is much better, since the program employs only first-order optics, with added aberrations. However, even under the best of circumstances—an actual channel resolution of 2×10^{-4} and the same scattered pion width of 4×10^{-3}—it will not be possible to distinguish the 0.6% scattered pions from the resolution function and radiation tail of the main peak. As long as the channel is tuned well enough to keep the percentage of slit-scattered pions small, this background may be ignored. Pion peaks can be fitted with an empirical resolution function that includes most slit-scattered pions. The remainder (about 10^{-4} of the height of the main peak) will blend with the large-energy-loss radiation tail and with the muons and slit-scattered pions produced in the spectrometer (described below).

The incident flux of protons is estimated to be about ten times as great as the incident flux of pions.[3] In the program, most protons were removed by the simulated proton separator. The remainder constituted an additional background of about 0.3% of the number of pions.

At 100 MeV, the muon contamination is about 35% of the number of pions. At 200 MeV it is 25%, and at 300 MeV it is 20%. This background will not be serious unless the spectrometer is positioned near 0° K. Seth has studied this case and has found that the background cannot be reduced even by

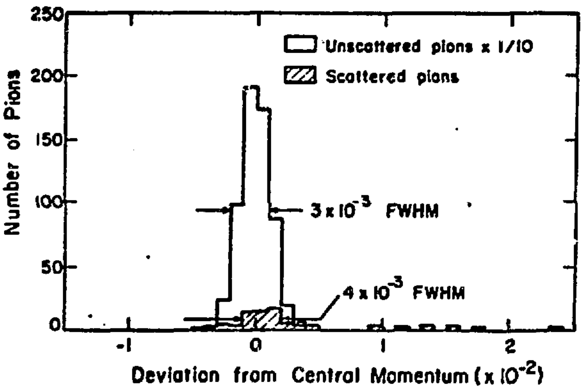

Fig. 5. Distribution of pions at the scattering target, projected to the focal plane of the spectrometer.

substantially closing the slits. This is because muons produced near the production target or any of the crossover points will be refocussed. Closing the slits located at the crossovers will remove these muons only in the same proportion that it will remove pions.

A simulation of the entrance to the pion channel (Fig. 6) was used to study the design of the fixed collimator. This water cooled collimator shields the first moveable jaws from the intense spray of particles emanating from the production target. The study predicted that the fixed slits should be of low Z material in order to reduce the number of particles scattered back into the opening between the moveable jaws. Since these jaws define the solid angle, the fixed slits which precede them should, ideally, do nothing more than serve as a heat shield. As a compromise between the need for low atomic number and high attenuation, the fixed collimator will be made of stainless steel.

Initially, at least, the channel will lack the fifth set of moveable jaws. Some or all of the other uranium jaws will be encased in steel to decrease the possibility of contamination. Even thin layers of steel will essentially determine the collimating properties of the jaws, as described in Part II. However, simulation of these conditions has shown no noticeable increase in the background of slit-scattered pions due to the use of steel rather than uranium. On the other hand, when one pair of curved jaws was temporarily replaced by flat jaws, the background rose by 25-30%.

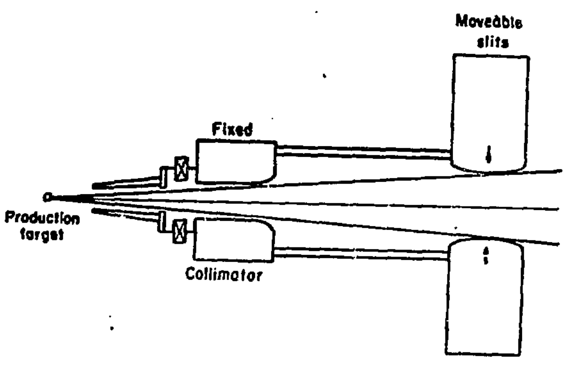

Fig. 6. Entrance to EPICS channel.

IV. EPICS SPECTROMETER SIMULATION

In addition to the background of slit-scattered pions already present at the scattering target, backgrounds will be generated by the decay and scattering of pions in the spectrometer. There are no special slits in the spectrometer to reduce these new backgrounds. However, multiwire helical chambers and thin scintillators will be positioned at the entrance and exit of the spectrometer dipoles. With these detectors, it will be possible to test each event to decide if its flight path is consistent with that expected from the magnet optics. Counting rates will probably be low enough (about 10^2/sec or less) to carry out these rejection tests on-line during the course of the experiment.

The first helical chamber and scintillator are situated at the image of the spectrometer triplet. To first order the information available here can be related to the scattering target by

$$x_1 = -x_T , \quad (1)$$

$$y_1 = \phi_T/5.048. \quad (2)$$

(x is the vertical, momentum-analyzing plane.) The second and third helical chambers provide x_2, y_2, θ_2, and ϕ_2 at the exit of the spectrometer. A second scintillator is positioned near these chambers, and the time difference between the second and first scintillators provides the time-of-flight between the entrance and exit of the spectrometer dipoles. To first order, the entrance and exit can be related by

$$\delta = .2384\ x_2 + .2384\ x_1 , \quad (3)$$

$$\theta_T = \theta_2 + 2.172\ x_1 - 2.172\ x_2 , \quad (4)$$

$$y_T = -.678\ y_2 - .288\ y_1 , \quad (5)$$

$$\phi_2 = -1.505\ y_2 - 3.526\ y_1 . \quad (6)$$

These equations suggest the following rejection tests:

1. First helical chamber must fire. From Equations 1 and 2, this is equivalent to testing x_T, ϕ_T to make sure they are reasonable.

2. Second and third helical chambers must fire. This automatically eliminates many muons and slit-scattered pions, at least in the initial configuration of the spectrometer, where the chambers span only half of the exit aperture.
3. Deviation from the central momentum δ (as calculated from Eq. 3) must lie within $\pm$ 5%, the range of the focal plane which the helical chambers initially span.
4. θ at the target (as calculated from Eq. 4) must lie within the acceptance of the triplet, about $\pm$ 100 mrad.
5. y at the target (as calculated from Eq. 5) must lie within the size of the target, $\pm$ 4.45 cm.
6. The calculated exit angle ϕ_2 (Eq. 6) must agree with the measured angle. Equation 6 can be rewritten as a test of ϕ_T, but in its present form it is perhaps more obvious that it is a very sensitive test for large angle pion decay.
7. The time-of-flight between the entrance and the exit of the spectrometer dipoles must be reasonable. For 200 MeV pions, this will be 25.0 ns.

The above rejection tests were simulated in the program in order to eliminate the backgrounds due to slit-scattered pions and muons. Table III lists the slits and lenses used to reproduce the spectrometer. Again, the optics are good to about 5%. Particles were chosen at the scattering target with their vertical position correlated to their momentum, as required by the dispersion of the channel, to within a small random error corresponding to a resolution of 2 x 10^{-4}. x_1, y_1, x_2, y_2, θ_2, and ϕ_2 were assigned random errors based on the chamber wire spacing and expected multiple scattering, as summarized in Table IV. The particle flight time was assigned an error of 1.0 nsec FWHM. Histograms of pions, slit scattered pions, and muons were calculated for each rejection test. Rejection criteria were set by the requirement that each rejected interval contain at least as many muons as pions. Under these conditions, it was possible to reject about 80% of the muons and 70% of the slit-scattered pions, at a loss of 3 or 4% of the total pions. An example of this is given in Table V.

The final ratio of muons to pions was about 3% at 100 MeV, 7% at 200 MeV, and 8% at 300 MeV. The variation is due primarily to the time-of-flight rejection test, which is more effective at lower energies. With a resolution of 1.0 nsec FWHM, time-of-flight was a useful test even at 200 MeV. A resolution of 2.0 nsec was also tried; this substantially increased the muon background even at 100 MeV. Since the spectrum of muon flight times overlaps the pion flight time, and extends to both longer and shorter times, it is important to achieve very good resolution on this measurement.

TABLE IIIA

EPICS SPECTROMETER SLITS

ZA, ZB define the position of the slit along the central trajectory. The half-aperture is A + ZSLP (Z - ZC) + $(Z - ZC)^2/2RC$.

Composition		ZA	ZB	ZC(X)	ZC(Y)	ZSLP(X)	ZSLP(Y)	RC(X)	RC(Y)	A(X)	A(Y)
1	Fe	92.10	104.80	104.80	104.80	0.0000	0.0000	0.000	0.000	15.240	6.985
2	Fe	104.80	159.60	159.60	159.60	0.0000	0.0000	0.000	0.000	17.500	14.000
3	Fe	159.60	204.60	204.60	204.60	0.0000	0.0000	0.000	0.000	17.500	14.000
4	Fe	204.60	249.60	249.60	249.60	0.0000	0.0000	0.000	0.000	14.000	17.500
5	Fe	249.60	294.60	294.60	294.60	0.0000	0.0000	0.000	0.000	14.000	17.500
6	Fe	294.60	339.60	339.60	339.60	0.0000	0.0000	0.000	0.000	17.500	14.000
7	Fe	339.60	499.30	499.30	499.30	0.0000	0.0000	0.000	0.000	17.500	14.000
8	Fe	499.30	640.70	499.30	499.30	0.2514	0.0000	0.000	0.000	11.300	11.000
9	Fe	640.70	650.70	650.70	650.70	0.0000	0.0000	0.000	10.000	58.420	8.890
10	Fe	650.70	726.40	726.40	726.40	0.0000	0.0000	0.000	0.000	58.420	8.890
11	Fe	726.40	766.50	766.50	766.50	0.0000	0.0000	0.000	0.000	58.420	8.890
12	Fe	766.50	776.50	766.50	766.50	0.0000	0.0000	0.000	10.000	58.420	8.890
13	Fe	776.50	841.50	841.50	841.50	0.0000	0.0000	0.000	0.000	38.740	9.208
14	Fe	841.50	906.50	906.50	906.50	0.0000	0.0000	0.000	0.000	38.740	9.208
15	Fe	906.50	916.50	916.50	916.50	0.0000	0.0000	0.000	10.000	58.420	8.890
16	Fe	916.50	956.60	956.60	956.60	0.0000	0.0000	0.000	0.000	58.420	8.890
17	Fe	956.60	1032.00	1032.00	1032.00	0.0000	0.0000	0.000	0.000	58.420	8.890
18	Fe	1032.00	1042.00	1032.00	1032.00	0.0000	0.0000	0.000	10.000	58.420	8.890
19	Fe	1042.00	1180.00	1042.00	1042.00	0.3064	0.0000	0.000	0.000	43.180	9.208

TABLE IIIB

EPICS SPECTROMETER LENSES

The lenses are positioned between slits N, N-1.

N	-1/fx	-1/fy	DX	DY
3	[illegible]	[illegible]	[illegible]	[illegible]
5	[illegible]	[illegible]	[illegible]	[illegible]
7	[illegible]	[illegible]	[illegible]	[illegible]
9	[illegible]	[illegible]	[illegible]	[illegible]
11	[illegible]	[illegible]	9.452	[illegible]
13	[illegible]	[illegible]	[illegible]	[illegible]
15	[illegible]	[illegible]	[illegible]	[illegible]
17	[illegible]	[illegible]	[illegible]	[illegible]
19	[illegible]	[illegible]	[illegible]	[illegible]

TABLE IV

RMS ERRORS ASSIGNED TO HELICAL CHAMBER DATA

	100 MeV	200 MeV	300 MeV
x_1 (helical direction)	.011 cm	.011 cm	.011 cm
y_1 (3 mm wire spacing)	.127 cm	.127 cm	.127 cm
x_2 (helical direction)	.011 cm	.011 cm	.011 cm
y_2 (3 mm wire spacing)	.127 cm	.127 cm	.127 cm
θ_2	3.3 mrad	1.8 mrad	1.3 mrad
ϕ_2	4.9 mrad	4.1 mrad	3.8 mrad

TABLE V

EPICS SPECTROMETER REJECTION TESTS

	Pass	Miss HC2	Miss HC1	Delta REJ	YT REJ	PHI2 REJ	THTT REJ	TOF REJ	FINAL Pass
Pions	12 119	45	18	50	41	220	55	69	11 705
Muons	4 239	1 332	31	895	1 305	2 445	708	471	854
Scattered Pions	89								24

An example of the use of rejection tests to decrease the background of muons and slit-scattered pions associated with 200 MeV elastically scattered pions. Many particles are rejected by more than one test.

Decreasing the y-direction wire spacing from 3 mm to 2 mm was also tried. This did not significantly improve the number of rejected muons.

Figures 7 and 8 illustrate the simulated momentum distribution of pions and muons at the focal plane after 200 MeV elastically scattered pions were traced through the spectrometer. Several satellite peaks and background tails were produced by the muons and slit-scattered pions. Since these effects should scale roughly with momentum, similar backgrounds will be associated with every inelastic peak in the pion spectrum.

Most of the muons which pass the rejection tests appear in three peaks:

Forward decays of pions early in the spectrometer yield muons that look like pions of 1 or 2% higher momentum. This produces a high energy muon tail and a small satellite peak (Fig. 7), about 2% of the area of the main peak, which may have to be allowed for during the analysis of weak inelastic peaks that lie at several percent higher energy than very strong inelastic peaks. At 100 MeV, time-of-flight eliminates this satellite peak.

Early backward decays of pions produce muons that look like pions of 40-50% lower momentum. This peak (Fig. 8) could interfere with quasi-elastic scattering experiments at low energies, but it is only about 0.1% of the elastic peak in area.

Very late forward decays of pions yield muons that are indistinguishable from pions. They produce a peak (Fig. 7) of about 2% of the area of the main peak and directly under it. Again, this background cannot be eliminated by line shape fitting of the main peak. However, since these muons were pions in

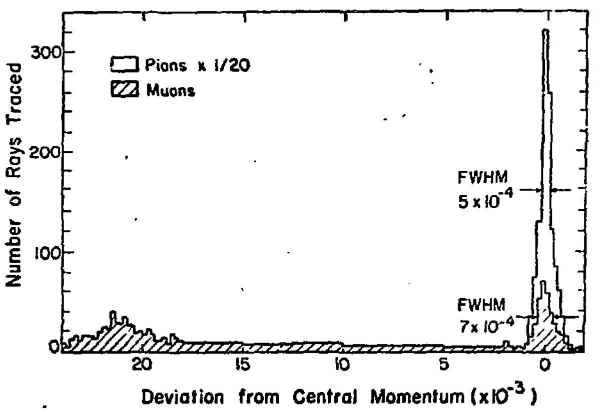

Fig. 7. Simulated momentum distribution of pions and muons at the focal plane of the EPICS spectrometer after 200 MeV elastic pion scattering. +2% to elastic region.

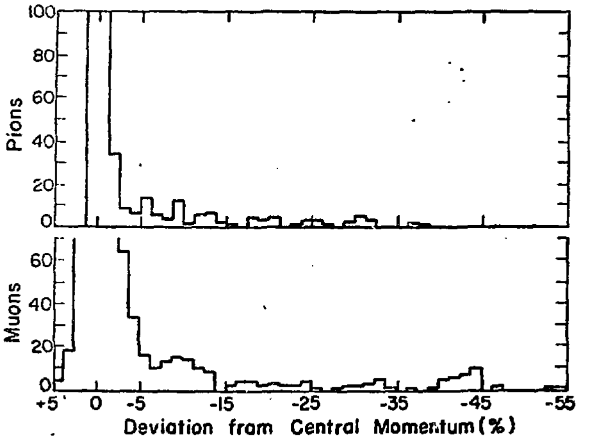

Fig. 8. Simulated momentum distribution of pions and muons at the focal plane of the EPICS spectrometer after 200 MeV elastic pion scattering. Elastic to -55% region.

the spectrometer dipoles, there is no error in including them with the main peak. The problem will arise in assigning an "effective flight path" to the spectrometer. This needs to be done whenever it is necessary to correct the measured pion cross section for the decay of pions between the scattering target and the focal plane.

The background tails due to muons and slit-scattered pions (Fig. 8) have been examined down to 55% of the elastic momentum—5 inelastic settings of the spectrometer. They remain small, 10^{-3} to 10^{-4} of the height of the elastic peak, over this region. There is no evidence for a pion "ghost peak" produced by elastic energy pions scattering from the walls of the vacuum chamber when the spectrometer current is set to sample inelastic events. Of course, a 10^{-3} or 10^{-4} background tail may be comparable in size to the radiation tail, but within the present statistics it appears to be a smooth background. The rejection tests have reduced its size by a factor of five.

Not simulated in the program is a lucite counter, situated behind the helical chambers, which will reject protons. However, the present results should serve as a reasonable prediction of the actual backgrounds and rejection tests. The data analysis program will base its rejection tests on calculations of x_T, y_T, θ_T, ϕ_T, and δ through fourth order. This should improve the tests, but on the other hand it will be more difficult to set the rejection criteria, since the actual identity of the particles will not be known.

References

1. Joseph F. Janni, "Calculations of Energy Loss, etc.," U.S.A.F. Technical Report No. AFWL-TR-65-150.

2. K. L. Brown and S. K. Howry, TRANSPORT/360, SLAC-91, p. 2-3.

3. D. Cochran et al., "Production of Charged Pions by 370-MeV Protons from Hydrogen and Selected Nuclei," Phys. Rev. D6, 11 (1972) 3085.

JJ:280(120)